



OPEN

# Dual-comb hyperspectral digital holography

Edoardo Vicentini<sup>1,2,3</sup>, Zhenhai Wang<sup>1,4</sup>, Kasper Van Gasse<sup>1,5</sup>, Theodor W. Hänsch<sup>1,6</sup> and Nathalie Picqué<sup>1</sup>✉

**Holography**<sup>1</sup> has always held special appeal as it is able to record and display spatial information in three dimensions<sup>2–10</sup>. Here we show how to augment the capabilities of digital holography<sup>11,12</sup> by using a large number of narrow laser lines at precisely defined optical frequencies simultaneously. Using an interferometer based on two frequency combs<sup>13–15</sup> of slightly different repetition frequencies and a lensless camera sensor, we record time-varying spatial interference patterns that generate spectral hypercubes of complex holograms, revealing the amplitudes and phases of scattered wave-fields for each comb line frequency. Advancing beyond multicolour holography and low-coherence holography (including with a frequency comb<sup>16</sup>), the synergy of broad spectral bandwidth and high temporal coherence in dual-comb holography opens up novel optical diagnostics, such as precise dimensional metrology over large distances without interferometric phase ambiguity, or hyperspectral three-dimensional imaging with high spectral resolving power, as we demonstrate with molecule-selective imaging of an absorbing gas.

With a set-up that involves merely the same simple hardware as that harnessed for dual-comb hyperspectral imaging<sup>17–20</sup>—two frequency-comb generators and a detector matrix—we take a new route to lensless scan-free three-dimensional (3D) profiling, suited to dimensional metrology of macroscopic and microscopic objects and to advanced optical sensing that combines spatial and spectral information.

In our technique for dual-comb holography (Fig. 1), a frequency-comb generator, called the object comb generator, emits a train of pulses at a repetition frequency  $f_{\text{rep}}$ . Its beam is either transmitted through or reflected by a 3D object. A beamsplitter combines the light scattered by the object with the beam of a second frequency-comb generator (called the reference) with a slightly different repetition frequency  $f_{\text{rep}} + \delta f_{\text{rep}}$ . The two trains of pulse wavefronts interfere at a fast lensless detector matrix and their interference signal at each matrix pixel is sampled as a function of time over a duration longer than  $1/\delta f_{\text{rep}}$ , while full interferometric coherence is maintained. The asynchrony of the two pulse trains enables interference between the object and reference waves over a range of optical delays that is limited only by the mutual coherence time of the interferometer, which can be longer than 1 s. However, as the interferometric signal recurs with an optical delay period of  $1/f_{\text{rep}}$ , the axial ambiguity range is  $c/f_{\text{rep}}$ , where  $c$  is the velocity of light.

As  $f_{\text{rep}}$  is typically on the order of hundreds of megahertz, the technique is suited to large-scale objects. At the end of the recording, as many time-domain interferograms as there are pixels are obtained (Fig. 2a). For each pixel, all spectral elements are acquired simultaneously by recording the interferogram. Each pixel

interferogram is Fourier transformed to reveal a complex spectrum of amplitude and phase (Fig. 2b). Even with an inline configuration, the holographic signal is spectrally separated from the non-interferometric zeroth-order signal and those of the twin holograms (complex-conjugate duplicates of the object field) because it is mapped in a different frequency range. This straightforward way to eliminate the blurring zeroth-order light and the twin image can be seen as analogous to phase-shifting holography<sup>21</sup>. Because the individual comb lines are resolved, as many holograms as there are comb lines are obtained. The amplitude and phase hologram at the well-defined optical frequency  $nf_{\text{rep}} + f_{\text{ceo}}$  (where  $n$  is an integer and  $f_{\text{ceo}}$  the carrier-envelope offset frequency) is mapped across the camera pixels at the radiofrequency  $n\delta f_{\text{rep}} + \delta f_{\text{ceo}}$  (where  $\delta f_{\text{ceo}}$  is the difference in the carrier-envelope offset frequencies of the two combs). The set of complex holograms at all comb frequencies provides a hologram hypercube (Fig. 2c). The reconstruction is then similar to that used in other techniques for digital holography. For a Fresnel hologram, the hologram is multiplied by a chosen reference wave and an inverse Fresnel transform computes the backpropagation at any depth of interest. Figure 2d shows reconstructed amplitude images, in reflection, of two spatially separated coins at different focal distances. Two amplitude and phase maps with a coin in focus are highlighted on the right. The reconstruction for an object in transmission is exemplified in Extended Data Fig. 1. Furthermore, the phase maps at different frequencies can be processed using well-established techniques of multiwavelength holography. With dual-comb interferometry<sup>13</sup>, however, a notable difference lies in the 100,000 frequencies that can potentially be measured simultaneously. Hierarchical phase unwrapping<sup>22</sup> could, for instance, be implemented on an unprecedented scale to extend—without increasing noise—the ambiguity range of the quantitative phase derivations, from the wavelength of one comb line to that corresponding to the comb repetition frequency. Moreover, another asset of the highly frequency-multiplexed character of dual-comb holography is the possibility of multimodal diagnostics. For example, if the object absorbs (or if an absorber is in the beam path), the amplitude of the reconstructed images also reveals its spectral absorption map, enabling identification and quantification. Unlike dual-comb hyperspectral imaging<sup>17–20</sup>, dual-comb digital holography provides 4D information (3D spatial and spectral dimensions).

Besides hyperspectral imaging, our technique might also be reminiscent—to readers familiar with frequency combs—of the single-photodetector dual-comb ranging technique, which combines time-of-flight (light detection and ranging; LIDAR) and interferometric distance measurements<sup>23</sup>. Holography and laser ranging are, however, substantially different in their principle and applications. These differences apply equally to dual-comb implementations.

<sup>1</sup>Max-Planck Institute of Quantum Optics, Garching, Germany. <sup>2</sup>Dipartimento di Fisica, Politecnico di Milano, Milan, Italy. <sup>3</sup>Istituto di Fotonica e Nanotecnologie, Consiglio Nazionale delle Ricerche, Milan, Italy. <sup>4</sup>Center for Combustion Energy, Department of Energy and Power Engineering, Tsinghua University, Beijing, China. <sup>5</sup>Photonics Research Group, INTEC, Ghent University-imec, Ghent, Belgium. <sup>6</sup>Faculty of Physics, Ludwig-Maximilian University of Munich, Munich, Germany. ✉e-mail: [nathalie.picque@mpq.mpg.de](mailto:nathalie.picque@mpq.mpg.de)

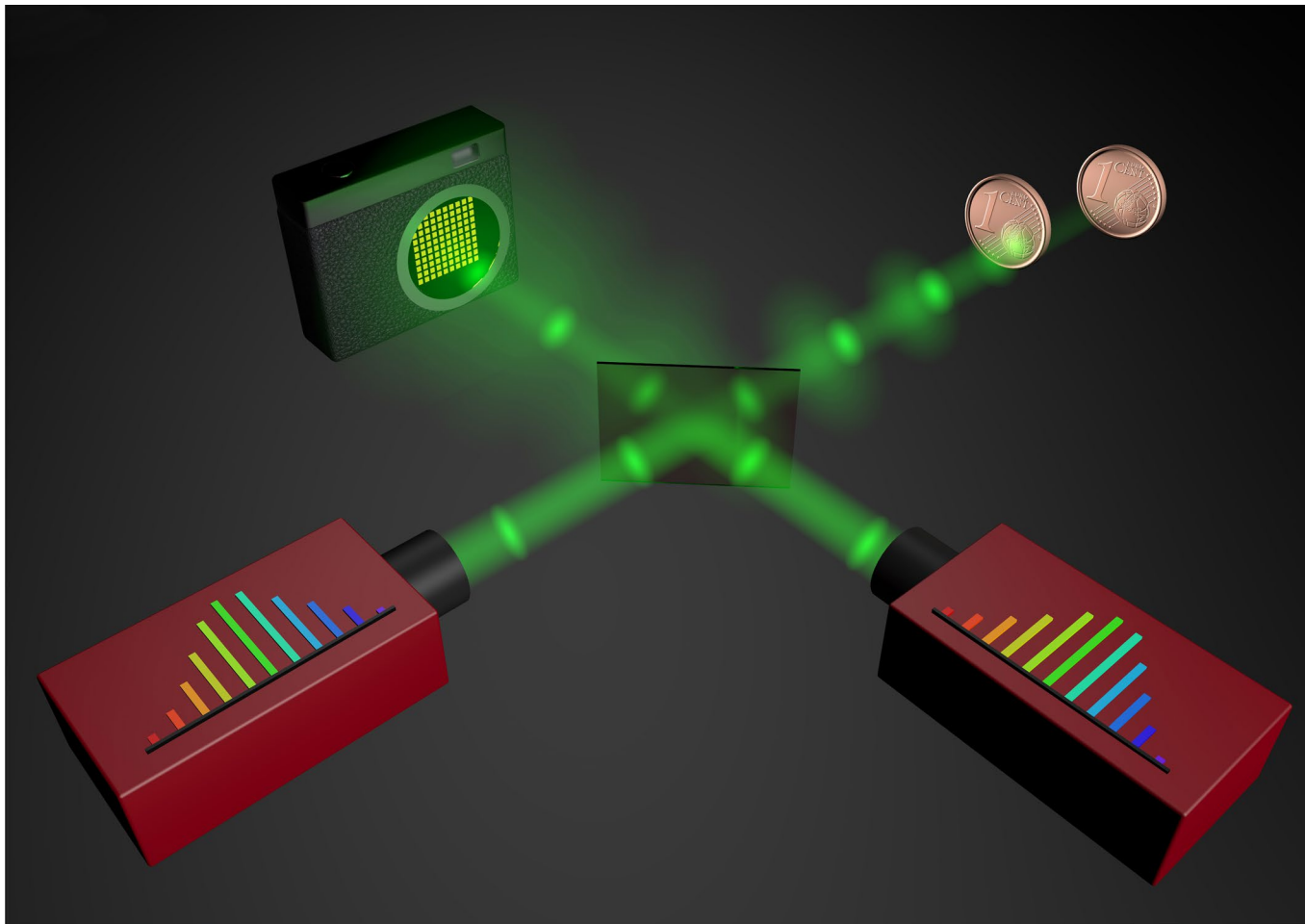


**Fig. 1 | Dual-comb digital holography.** The regular train of pulses of a frequency-comb generator illuminates an object (here two coins in reflection). The wave scattered by the object spatially and temporally interferes with that of a reference comb at a lensless detector matrix. Analysis of the temporal and spatial interference restores holograms and their reconstructed images (Fig. 2).

In particular, LIDAR relies on the assumption that there is an unambiguous pointwise correspondence between the object and the detector pixel. LIDAR approaches that exploit a detector matrix (or multiplexing techniques) parallelize this hypothesis. In holography, on the other hand, the complex object wave is scattered and spatially interferes with the reference wave. The reconstruction of the hologram analyses this 2D interference pattern to restore the complex object field, with its depth and parallax. Digital holography is a uniquely powerful lensless and scan-free 3D imaging method through linear and nonlinear<sup>2,3</sup> media at the micro- and nanoscales, possibly at high temporal resolution<sup>4</sup>. Its applications<sup>5,11,12</sup> include optical contouring and deformation measurements, wavefront sensing, 3D profiling over relatively short distances (compared with the hundreds of kilometres demonstrated by LIDAR techniques), microscopy and nanoscopy for life science<sup>6,7</sup>, particle imaging velocimetry, tomography and laser speckle contrast imaging, as well as the generation of complex 3D wavefronts through computer-generated holograms in fields such as optogenetics<sup>8</sup>, data storage<sup>9</sup> or near-eye displays for virtual and augmented reality<sup>10</sup>.

We performed an experimental proof-of-principle of inline Fresnel dual-comb holography in the near-infrared telecommunication spectral region (Fig. 3a and Methods). Our slow InGaAs detector matrix (320 Hz frame rate) dictated a small number of comb lines and long measurement times, and it influenced the choice of a dual-comb interferometer based on electro-optic frequency comb generators. We generated two frequency combs of slightly

different repetition frequencies,  $f_{\text{rep}}$  for the object comb and  $f_{\text{rep}} + \delta f_{\text{rep}}$  for the reference comb, by dividing the output of a continuous-wave laser with a beam splitter, and sending each beam through an electro-optic amplitude modulator producing pulses of about 50 ps. The repetition frequency of the object comb and the difference in repetition frequencies were  $f_{\text{rep}} = 500$  MHz,  $\delta f_{\text{rep}} = 1$  Hz (Figs. 3b and 4) or  $f_{\text{rep}} = 1,000$  MHz,  $\delta f_{\text{rep}} = 2$  Hz (Figs. 2 and 5). We actually achieved broader spectral coverage by starting with two independent continuous-wave lasers of different frequencies<sup>24</sup> (here around 195 THz). Their outputs were superimposed so that each modulator produced two spectrally separated frequency combs. These two combs do not need to be mutually coherent and we did not attempt to achieve this. Each of the four modulator input beams was fine-tuned with an acousto-optic frequency shifter, enabling the two dual-comb spectra to be mapped within the camera sampling bandwidth, at 40 Hz and 120 Hz respectively. A beam splitter combined the scattered waves with the beam of the reference comb generator. The object and reference waves beat on the lensless InGaAs detector matrix of  $320 \times 256$  pixels.

In a first experiment, the 3D character of the technique was exemplified. The objects were two coins (€1 (€)), 9 cm apart (Fig. 2 and Methods). The interferogram hypercube was used to generate a hologram hypercube and then to reconstruct amplitude and phase maps, following the general procedure explained in Fig. 2. Amplitude images show one coin in focus when the other is out of focus (Fig. 2d and Supplementary Video 1).

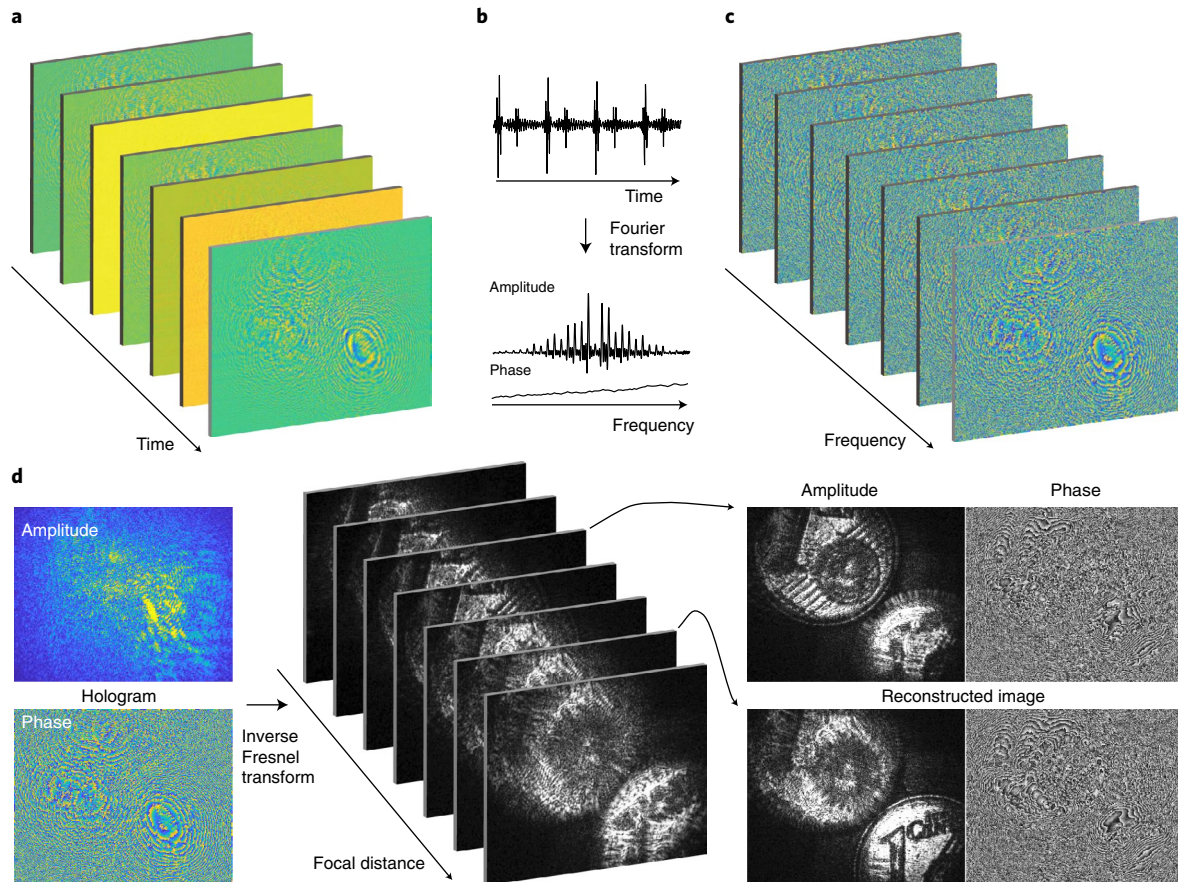


**Fig. 2 | Reconstruction of dual-comb holographic amplitude and phase maps.** **a**, The frames of the interference between the object and reference waves are sampled as a function of time on a detector matrix. The object comprises two spatially separated coins. As many time-domain interferograms as there are pixels are measured. **b**, For each pixel, each interferogram is Fourier transformed to reveal frequency-domain amplitude and phase spectra with resolved comb lines. **c**, The hologram hypercube includes as many complex holograms as there are comb lines: at a given frequency, the hologram includes the amplitude and phase of the spectrum across all detector pixels. **d**, For each frequency, an inverse Fresnel transform of the holograms generates amplitude and phase images over the entire range of focal distances. Here, two focused images with their phase maps are highlighted. The multiple phase maps will enable the phase to be unwrapped and the three-dimensional structure of the object to be rendered (Fig. 5).

A second experiment illustrated the capabilities of our technique for multimodal diagnostics. The two continuous-wave lasers emitted at optical frequencies of 195.353 THz and 195.725 THz, respectively. The object beam was reflected and scattered by a coin (¢1) and passed through 40 cm of ammonia vapour in air in each direction. An interferogram hypercube, consisting of 81,920 pixel interferograms, was measured over a period of 91 s. The Fourier transform of the pixel interferograms led to amplitude (Fig. 3b) and phase spectra with 100 resolved comb lines for each pixel. Each dual-comb hologram spectrum showed two downconverted combs, centred at 40 Hz (for the combs centred at 195.353 THz) and 120 Hz (for the combs centred at 195.725 THz) respectively. Dual-comb holography offers high-quality complex images at any focal distance: an inverse Fresnel transform<sup>25</sup>, assuming a plane-wave reference wave, computed a set of amplitude and phase images (Extended Data Fig. 2a) for 100 different optical frequencies, at any desired depth. At the focus for the coin (a focusing distance of 69.7 cm), two amplitude images, one outside absorption and one within an NH<sub>3</sub> absorption line, show excellent agreement (Fig. 4); but, as expected, the latter is strongly attenuated. For each of the 81,920 pixels, the amplitude variations across the comb line frequencies provide the absorption along the beam path. The NH<sub>3</sub> absorption spectrum of pixel (160,128) shows good agreement with a spectrum adjusted from line parameters available in the high-resolution transmission molecular absorption (HITRAN) database (Fig. 4), demonstrating

the potential of our technique for concentration measurements. As is usual in digital holography, the images can be reconstructed even in the presence of faulty detector pixels (Extended Data Fig. 2).

The benefits of the large frequency multiplexing are not limited to the possibility of multimodal diagnostics. The ambiguity range of the holographic measurements is also greatly enhanced, as illustrated in a third experiment dedicated to the 3D reconstruction of the depth map. Using multifrequency phase unwrapping, limited to the phase images of the comb lines that do not experience absorption by the sample, a quantitative 3D phase map was reconstructed (Fig. 5 and Supplementary Video 1). The absorption feature is shown in Extended Data Fig. 3.

Dual-comb holography will be dramatically improved when it is moved to the range of visible and near-infrared wavelengths, down to 1 μm. Much faster cameras, based on silicon technology are commercially available with a greater number of pixels and a larger sensor. Rates as high as  $3 \times 10^5$  frames per second are achievable at 600 × 400 pixel sizes. Their use will make it possible to increase the number of comb lines, the span, the measurement speed and the spatial resolution, enabling powerful implementations with self-referenced fibre-based frequency comb synthesizers. Mapping the dual-comb signal at higher frequencies will be more immune to technical noise (which is our main limitation at present). Broader spans will be crucial to obtaining a wide and uniform set of synthetic frequencies and will improve

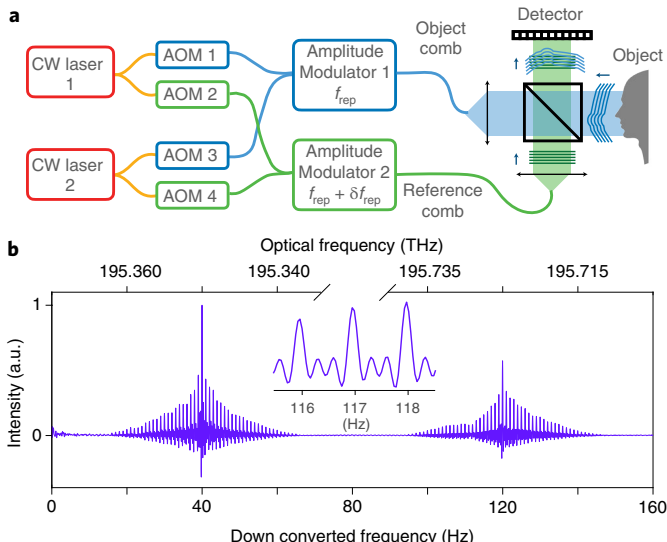


**Fig. 3 | Dual-comb interferometry for inline Fresnel holography.** **a**, Set-up for implementation with electro-optic modulators. Two continuous-wave (CW) lasers feed two amplitude modulators driven at slightly different repetition frequencies. Each modulator generates two combs of the same line spacing but with independently adjustable centre frequencies. The acousto-optic modulators (AOMs) frequency shift the downconverted dual-comb spectra within the detector-matrix bandwidth. The object comb wave is scattered by the object and interferes at a detector matrix with the reference comb wave. **b**, Dual-comb amplitude spectrum of pixel (160,128) of about 100 lines. The inset shows three individual comb lines. The amplitude and phase of the complex spectrum at one comb line position across all pixels generate the complex hologram at a given frequency. a.u., arbitrary units.

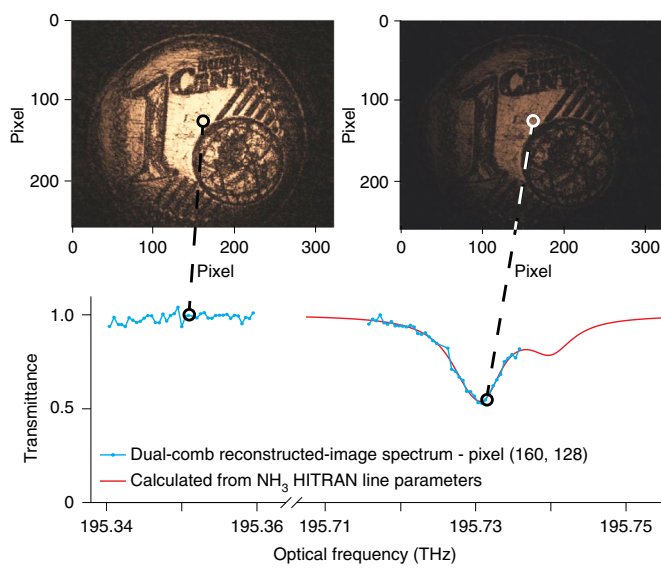
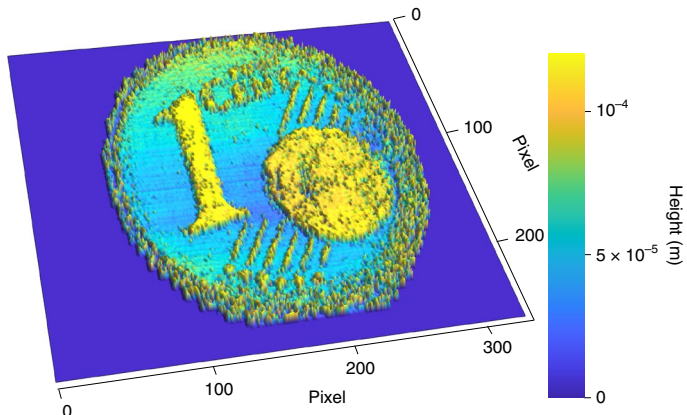


**Fig. 4 | Illustration of the reconstruction of an experimental dual-comb hologram hypercube.** The object is a coin, and the experiment was conducted in the presence of an absorber (ammonia vapour) in the object beam path. Top: reconstructed amplitude images of the coin in focus (at 697 mm) for frequencies of 195.351 THz (left) and 195.731 THz (right). Bottom: each of the 81,920 pixels of the reconstructed amplitude image cube can be plotted as a high-resolution spectrum, such as that plotted here for pixel (160,128). The spectrum reveals<sup>30</sup> the blended transition  $P_P(5,3)a$  of the  $\nu_1 + \nu_3$  band in  $^{14}\text{NH}_3$ , measured with a sufficiently high signal-to-noise ratio to enable precise concentration measurements.



the phase unwrapping procedure. Furthermore, broad spans will facilitate the simultaneous realization of several types of optical diagnostic with the same instrument, such as the hyperspectral 3D imaging with high spectral resolving power explored here. Although absorption is usually weak in the visible range, non-linear dual-comb spectroscopy exploiting, for example, coherent Raman effects<sup>26</sup> might provide access to fundamental vibrational bands. An interferometer of high mutual coherence based on two frequency-comb synthesizers fully referenced to a radiofrequency clock, as is conveniently available from fibre-laser systems<sup>13</sup>, will be key to exploring the frontiers of our technique in terms of precision and accuracy and will enable dual-comb holography to evolve into a tool of dimensional metrology.

In the longer term, progress to camera technology may enable extension of the technique to spectral regions such as the mid-infrared—or even the terahertz—range. This is hampered at present by a number of technical challenges. For example, the slower frame rates of camera sensors in these regions requires to down-convert the dual-comb signal in a range of low frequencies, which is prone to stronger intensity noise, and to harness interferometers of longer mutual coherence times. Nevertheless, the characterization of visually opaque objects is a particularly exciting prospect. Building on existing instrumentation in the long-wavelength range, both for digital holography<sup>27</sup> and for frequency comb generators<sup>13,28,29</sup>, further applications may also emerge in quality control or biomedical sensing, for example.

Dual-comb interferometers already show intriguing potential in spectroscopy<sup>13</sup>, spectro-imaging<sup>17,26</sup> and ranging<sup>23</sup>. Their unique combination of broad spectral bandwidth, long temporal coherence and multi-heterodyne readout offers holography a distinctive host of powerful features—frequency multiplexing, accuracy, precision, speed, large ambiguity range—that is likely to conquer new frontiers in scan-free wavefront reconstruction and 3D metrology.

## Online content

Any methods, additional references, Nature Research reporting summaries, source data, extended data, supplementary information, acknowledgements, peer review information; details of author contributions and competing interests; and statements of data and code availability are available at <https://doi.org/10.1038/s41566-021-00892-x>.

Received: 2 May 2021; Accepted: 8 September 2021;  
Published online: 22 November 2021

## References

1. Gabor, D. A new microscopic principle. *Nature* **161**, 777–778 (1948).
2. Barsi, C., Wan, W. & Fleischer, J. W. Imaging through nonlinear media using digital holography. *Nat. Photon.* **3**, 211–215 (2009).
3. Tsang, M., Psaltis, D. & Omenetto, F. G. Reverse propagation of femtosecond pulses in optical fibers. *Opt. Lett.* **28**, 1873–1875 (2003).
4. Tikan, A., Bielawski, S., Szwaj, C., Randoux, S. & Suret, P. Single-shot measurement of phase and amplitude by using a heterodyne time-lens system and ultrafast digital time-holography. *Nat. Photon.* **12**, 228–234 (2018).
5. Cuche, E., Emery, Y. & Montfort, F. One-shot analysis. *Nat. Photon.* **3**, 633–635 (2009).
6. Rosen, J. & Brooker, G. Non-scanning motionless fluorescence three-dimensional holographic microscopy. *Nat. Photon.* **2**, 190–195 (2008).
7. Cotte, Y. et al. Marker-free phase nanoscopy. *Nat. Photon.* **7**, 113–117 (2013).
8. Pégard, N. C. et al. Three-dimensional scanless holographic optogenetics with temporal focusing (3D-SHOT). *Nat. Commun.* **8**, 1228 (2017).
9. Barbastathis, G. & Psaltis, D. in *Holographic Data Storage Springer Series in Optical Sciences* (eds Coufal, H. J. et al.) 21–62 (Springer, 2000); [https://doi.org/10.1007/978-3-540-47864-5\\_2](https://doi.org/10.1007/978-3-540-47864-5_2)
10. Shi, L., Li, B., Kim, C., Kellnhofer, P. & Matusik, W. Towards real-time photorealistic 3D holography with deep neural networks. *Nature* **591**, 234–239 (2021).
11. Poon, T.-C. & Liu, J.-P. *Introduction to Modern Digital Holography: With Matlab* (Cambridge Univ. Press, 2014); <https://doi.org/10.1017/CBO9781139061346>
12. Schnars, U., Falldorf, C., Watson, J. & Jüptner, W. *Digital Holography and Wavefront Sensing* (Springer, 2015); <https://doi.org/10.1007/978-3-662-44693-5>
13. Picqué, N. & Hänsch, T. W. Frequency comb spectroscopy. *Nat. Photon.* **13**, 146–157 (2019).
14. Hänsch, T. W. Nobel lecture: passion for precision. *Rev. Mod. Phys.* **78**, 1297–1309 (2006).
15. Udem, T., Holzwarth, R. & Hänsch, T. W. Optical frequency metrology. *Nature* **416**, 233–237 (2002).
16. Körner, K. et al. Short temporal coherence digital holography with a femtosecond frequency comb laser for multi-level optical sectioning. *Opt. Express* **20**, 7237–7242 (2012).
17. Martín-Mateos, P., Khan, F. U. & Bonilla-Manrique, O. E. Direct hyperspectral dual-comb imaging. *Optica* **7**, 199–202 (2020).
18. Khan, F. U., Guarnizo, G. & Martín-Mateos, P. Direct hyperspectral dual-comb gas imaging in the mid-infrared. *Opt. Lett.* **45**, 5335–5338 (2020).
19. Voumard, T. et al. AI-enabled real-time dual-comb molecular fingerprint imaging. *Opt. Lett.* **45**, 6583–6586 (2020).
20. Vicentini, E. et al. High-spectral-resolution imaging spectroscopy with a dual-comb interferometer. In *Frontiers in Optics/Laser Science* (eds Mazzali, B. et al.) LTu2F.3 (Optical Society of America, 2020); <https://doi.org/10.1364/LS.2020.LTu2F.3>
21. Yamaguchi, I. & Zhang, T. Phase-shifting digital holography. *Opt. Lett.* **22**, 1268–1270 (1997).
22. Gass, J., Dakoff, A. & Kim, M. K. Phase imaging without  $2\pi$  ambiguity by multiwavelength digital holography. *Opt. Lett.* **28**, 1141–1143 (2003).
23. Coddington, I., Swann, W. C., Nenadovic, L. & Newbury, N. R. Rapid and precise absolute distance measurements at long range. *Nat. Photon.* **3**, 351–356 (2009).
24. Shams-Ansari, A. et al. An integrated lithium-niobate electro-optic platform for spectrally tailored dual-comb spectroscopy. Preprint at <https://arxiv.org/abs/2003.04533> (2020).
25. Latychevskaia, T. & Fink, H.-W. Practical algorithms for simulation and reconstruction of digital in-line holograms. *Appl. Opt.* **54**, 2424–2434 (2015).
26. Ideguchi, T. et al. Coherent Raman spectro-imaging with laser frequency combs. *Nature* **502**, 355–358 (2013).
27. Locatelli, M. et al. Real-time terahertz digital holography with a quantum cascade laser. *Sci Rep.* **5**, 13566 (2015).
28. Consolino, L. et al. Fully phase-stabilized quantum cascade laser frequency comb. *Nat. Commun.* **10**, 2938 (2019).
29. Schliesser, A., Picqué, N. & Hänsch, T. W. Mid-infrared frequency combs. *Nat. Photon.* **6**, 440–449 (2012).
30. Sung, K. et al. Extended line positions, intensities, empirical lower state energies and quantum assignments of NH<sub>3</sub> from 6300 to 7000cm<sup>-1</sup>. *J. Quant. Spectrosc. Radiat. Transfer* **113**, 1066–1083 (2012).

**Publisher's note** Springer Nature remains neutral with regard to jurisdictional claims in published maps and institutional affiliations.



**Open Access** This article is licensed under a Creative Commons Attribution 4.0 International License, which permits use, sharing, adaptation, distribution and reproduction in any medium or format, as long as you give appropriate credit to the original author(s) and the source, provide a link to the Creative Commons license, and indicate if changes were made. The images or other third party material in this article are included in the article's Creative Commons license, unless indicated otherwise in a credit line to the material. If material is not included in the article's Creative Commons license and your intended use is not permitted by statutory regulation or exceeds the permitted use, you will need to obtain permission directly from the copyright holder. To view a copy of this license, visit <http://creativecommons.org/licenses/by/4.0/>.

© The Author(s) 2021

## Methods

### Dual-comb interferometer for proof-of-principle demonstration of inline Fresnel holography.

The reported demonstration of dual-comb hyperspectral digital holography made expedient use of equipment already available in our laboratory. The experimental choices were pragmatically based on the limitations of these tools.

The main limitation on our experiment in the near-infrared telecommunications region was imposed by the slow 320 Hz frame rate of the detector matrix, a lensless InGaAs thermo-electrically cooled camera of  $320 \times 256$  (81,920) pixels. At such slow frame rates, it is difficult to accommodate a large number of comb lines in dual-comb interferometry, and it is challenging to maintain the mutual coherence of two frequency combs over the necessary long observation times. We therefore resorted to modulator-based combs with fewer than 100 comb lines, but excellent passive mutual coherence<sup>31,32</sup>. The few previous experiments combining detector matrices and dual-comb interferometers have all made use of a double acousto-optic-frequency-shifter scheme<sup>17–20</sup>, where the two combs are shifted by a slightly different radiofrequency, enabling the downconverted comb to be centred at frequencies on the order of tens of hertz. To increase the effective spectral span, we employed two sub-combs in each frequency comb, separated in frequency by several hundred gigahertz, as has been done before in spectrally tailored dual-comb spectroscopy with thin-film lithium-niobate-on-insulator electro-optic micro-rings<sup>24</sup>. By acousto-optically fine-tuning the carrier frequencies of each of the four combs, we could freely shift the dual-comb interference frequencies so that the signals from both downconverted sub-combs fell within the detector-matrix bandwidth and aliasing was avoided.

As shown in Fig. 3a, we started with two fibre-coupled broadly tunable free-running continuous-wave lasers with narrow linewidths, emitting around 195 THz. Each continuous-wave laser beam was split into two beams, each of which was sent into an acousto-optic modulator (AOM), which acted as a frequency shifter. Modulator AOM*i* (where *i* = 1, 2, 3, 4) was driven at  $\delta f_i$ , where  $\delta f_1 = 25.0$  MHz,  $\delta f_2 = 25.0$  MHz + 40 Hz,  $\delta f_3 = 40.0$  MHz,  $\delta f_4 = 40.0$  MHz + 120 Hz. The beams at frequencies  $f_1 + \delta f_1$  and  $f_2 + \delta f_2$  were combined and sent into an electro-optic amplitude modulator (Amplitude Modulator 1). Driven by a synthesizer and a pulse generator, Amplitude Modulator 1 generated a train of 50 ps pulses at  $f_{\text{rep}} = 1,000$  MHz (Figs. 2 and 5) or 500 MHz (Figs. 3b and 4). Similarly, the beams at frequencies  $f_1 + \delta f_3$  and  $f_2 + \delta f_4$  were sent into Amplitude Modulator 2. Amplitude Modulator 2 also generated a train of 50 ps pulses at the slightly different radiofrequency  $f_{\text{rep}} + \delta f_{\text{rep}} = 1,000$  MHz + 2 Hz (Figs. 2 and 5) or 500 MHz + 1 Hz (Figs. 3b and 4). The fibre-coupled amplitude modulators had a frequency bandwidth of 20 GHz and an extinction ratio of 40 dB at 1,550 nm. At the output of Amplitude Modulator 1, two spectrally separated sub-combs were generated, centred at the optical frequencies  $f_1 + \delta f_1$  and  $f_2 + \delta f_2$ , respectively. These two sub-combs, which formed the object comb, had a line spacing equal to  $f_{\text{rep}}$  and count about 50 lines each when  $f_{\text{rep}} = 500$  MHz (about 25 lines when  $f_{\text{rep}} = 1,000$  MHz). As the two sub-combs were generated from two independent free-running continuous-wave lasers, they were expected to show poor mutual coherence, which did not matter in our experiment. The output of Amplitude Modulator 2 was similar, with its corresponding parameters, and generated the reference comb with two sub-combs.

At the output of the amplitude modulators, the beams of the object and reference combs were collimated in free space to a diameter slightly larger than that of the detector matrix. The beam of the object comb was transmitted through or reflected and scattered onto an object. Figures 2–5 display results where the scattered light was reflected by the object, whereas Extended Data Fig. 1 illustrates the reconstruction of holograms for an object in transmission. The object and reference waves were then combined in a beam splitter cube and beat on a detector matrix sensor. The pixel size of the sensor was  $30 \times 30 \mu\text{m}^2$  and its dynamic range was 14 bits. Although the frame rate was 320 Hz, the integration time per frame was set to  $10^{-4}$  s to prevent saturation of the camera sensor. A frame-grabber card captured the sensor frames and streamed them to the hard drive of a computer. All of the electronic instruments (synthesizers, camera and so on) in the experiment were synchronized to a 10 MHz clock signal.

Two downconverted sub-combs with line spacing  $\delta f_{\text{rep}}$  were generated in the detector signal: one sub-comb centred at  $\delta f_2 - \delta f_1 = 40$  Hz, the other sub-comb centred at  $\delta f_4 - \delta f_3 = 120$  Hz. For each matrix pixel, the time-domain pixel interferogram was Fourier transformed and further processed as described in Fig. 2. The spectra confirmed that the optical sub-combs, generated from the same continuous-wave laser and different amplitude modulators, showed excellent mutual coherence, here longer than 10 s, owing to the shared optical carrier.

**Recording and reconstruction conditions.** In Fig. 2, the two continuous-wave lasers emitted at respective frequencies of  $f_1 = 195.353$  THz and  $f_2 = 195.420$  THz. The object comb line spacing was  $f_{\text{rep}} = 1,000$  MHz and the difference in repetition frequencies was  $\delta f_{\text{rep}} = 2$  Hz. The object comb and the reference comb each included about 50 lines. In Fig. 2, the objects were two coins at two different positions along the beam axis, separated by 9 cm, and slightly displaced laterally. A telescope, in the object beam path, was made of two spherical mirrors. It magnified the incoming object beam fivefold before it reached the two coins (and demagnified the exiting

object waves by the same factor). An interferometric hypercube, consisting of 81,920 pixel interferograms, was measured within a total measurement time of 3.5 s (Supplementary Video 1). After being Fourier transformed, amplitude and phase holograms were obtained, as illustrated in Fig. 2 and Supplementary Video 1. The computation of the holograms and the reconstruction of the images and phase maps were performed using a MATLAB program.

In Fig. 3b and Fig. 4, the two continuous-wave lasers emitted at respective frequencies of  $f_1 = 195.353$  THz and  $f_2 = 195.725$  THz. The object comb line spacing was  $f_{\text{rep}} = 500$  MHz and the difference in repetition frequencies was  $\delta f_{\text{rep}} = 1$  Hz. The object comb and the reference comb each included about 100 lines. The object was a ¢1 coin, which scattered the reflected light. Before and after the reflection onto the coin, the object waves went through a box, with holes to let the light in and out on each side and ammonia water at the bottom, and through a telescope made of two spherical mirrors that magnified the incoming object beam about twofold before it reached the coin (and demagnified the exiting object waves by the same factor). An interferogram hypercube consisting of 81,920 pixel interferograms was measured within 7 s. After being Fourier transformed, thirteen spectral hypercubes were averaged, leading to a total measurement time of 91 s.

In Fig. 5, the two continuous-wave lasers emitted at respective frequencies of  $f_1 = 194.923$  THz and  $f_2 = 195.725$  THz. The object comb line spacing was  $f_{\text{rep}} = 1,000$  MHz and the difference in repetition frequencies was  $\delta f_{\text{rep}} = 2$  Hz. The object comb and the reference comb each included about 50 lines. The object (¢1 coin) and absorbing sample (ammonia water) were the same as for the data in Fig. 4. The telescope magnified 2.5-fold. The interferogram hypercube, consisting of 81,920 pixel interferograms, was measured within 3.5 s and 27 averages were performed in the spectral domain, leading to a total measurement time of 94.5 s. The same ammonia line as in Fig. 4, sampled at 1,000 MHz line spacing, is shown in Extended Data Fig. 3 for pixel (160,128).

The reconstruction of the images and phase maps from the holograms (Figs. 2 and 4 and Supplementary Video 1) assumed a plane-wave reference wave and used the angular spectrum method<sup>11</sup>. We followed the reconstruction procedure described in the tutorial article<sup>25</sup>. To render the 3D profile of a coin (Fig. 5 and Supplementary Video 1) from the phase maps, hierarchical phase unwrapping, as described in<sup>26</sup>, was implemented. Nevertheless, the result appeared noisy in this proof-of-principle demonstration: this is mainly attributed to technical noise generated by the camera and by the employed comb generators. The camera randomly lost its synchronization with the clock signal during the acquisitions, which is likely to generate phase noise (extensive interactions with the manufacturer did not provide any solutions or improvements). In addition, the average integrated relative intensity noise power spectral density of each comb source was measured to be  $-90$  dBc Hz<sup>-1</sup> in the detection band from 2–160 Hz, varying from  $-70$  dBc Hz<sup>-1</sup> at 2 Hz to  $-93$  dBc Hz<sup>-1</sup> at 160 Hz. The technical relative intensity noise is currently the main source of noise in our signal-to-noise ratio estimates. Mapping dual-comb spectra in a low frequency range (here < 160 Hz), compared with the usual tens or hundreds of megahertz<sup>13</sup>, represents a newly explored technical regime that will be subject to further investigation and improvements. As discussed, major progress is expected from the use of dedicated, faster cameras that will also be able to accommodate a greater number of comb lines over a broader span, improving the phase unwrapping.

## Data availability

The data used to produce the plots within this article are available at Edmond, the Open Access Max Planck Research Data Repository, at <https://doi.org/10.17617/3.63>.

## Code availability

No original algorithms or codes have been developed for this article. The MATLAB program used for processing the data is nevertheless available from the corresponding author on reasonable request.

## References

31. Long, D. A. et al. Multiheterodyne spectroscopy with optical frequency combs generated from a continuous-wave laser. *Opt. Lett.* **39**, 2688–2690 (2014).
32. Millot, G. et al. Frequency-agile dual-comb spectroscopy. *Nat. Photon.* **10**, 27–30 (2016).

## Acknowledgements

We thank K. Linner for technical support. Funding from the Max-Planck Society, the Carl-Friedrich von Siemens Foundation, the Max-Planck Fraunhofer cooperation programme, the Flemish Research Council (postdoctoral fellowship number 12ZB520N, K.V.G.) and the China Scholarship Council (scholarship, Z.W.) is gratefully acknowledged.

## Author contributions

E.V. performed the experiments, assisted by Z.W. E.V. processed the data, assisted by K.V.G. E.V., N.P. and T.W.H. analysed the results. N.P. conceived the project and supervised the work. N.P., E.V. and T.W.H. designed the set-up. N.P. drafted the

manuscript with input from T.W.H. and E.V. All authors discussed the results and approved the manuscript

**Funding**

Open access funding provided by Max Planck Society.

**Competing interests**

The authors declare no competing interests.

**Additional information**

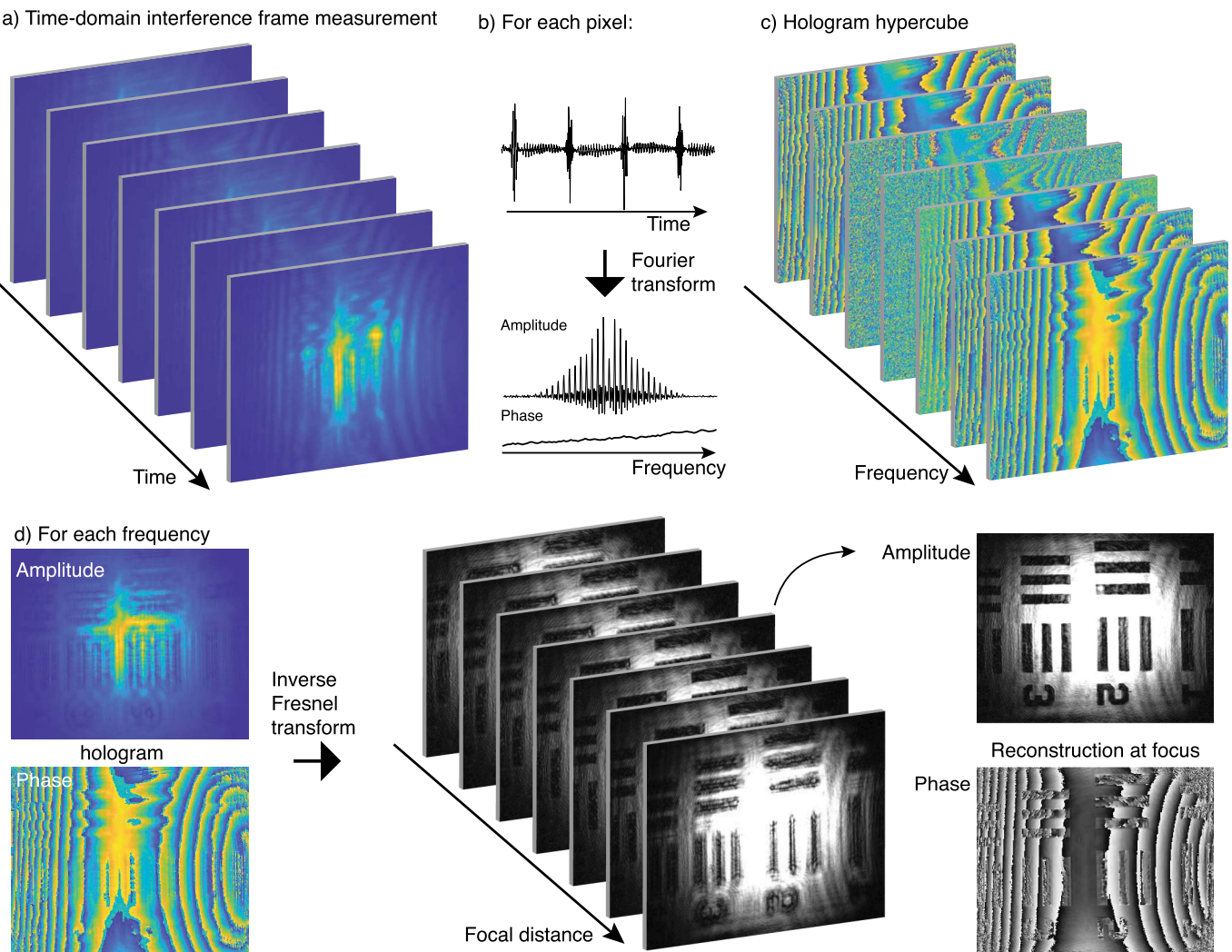
**Extended data** is available for this paper at <https://doi.org/10.1038/s41566-021-00892-x>.

**Supplementary information** The online version contains supplementary material available at <https://doi.org/10.1038/s41566-021-00892-x>.

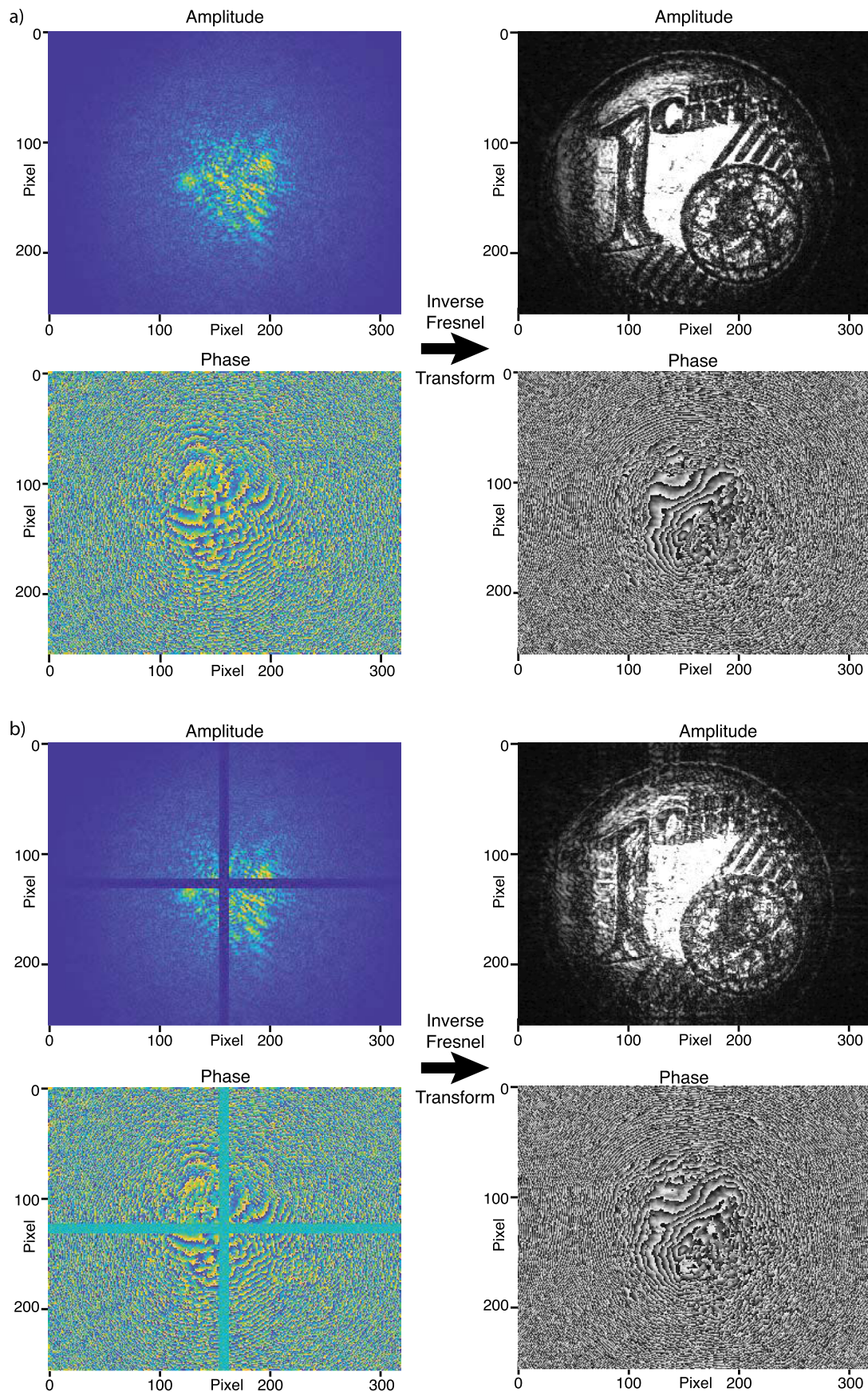
**Correspondence and requests for materials** should be addressed to Nathalie Picqué.

**Peer review information** *Nature Photonics* thanks David Burghoff and the other, anonymous, reviewer(s) for their contribution to the peer review of this work.

**Reprints and permissions information** is available at [www.nature.com/reprints](http://www.nature.com/reprints).

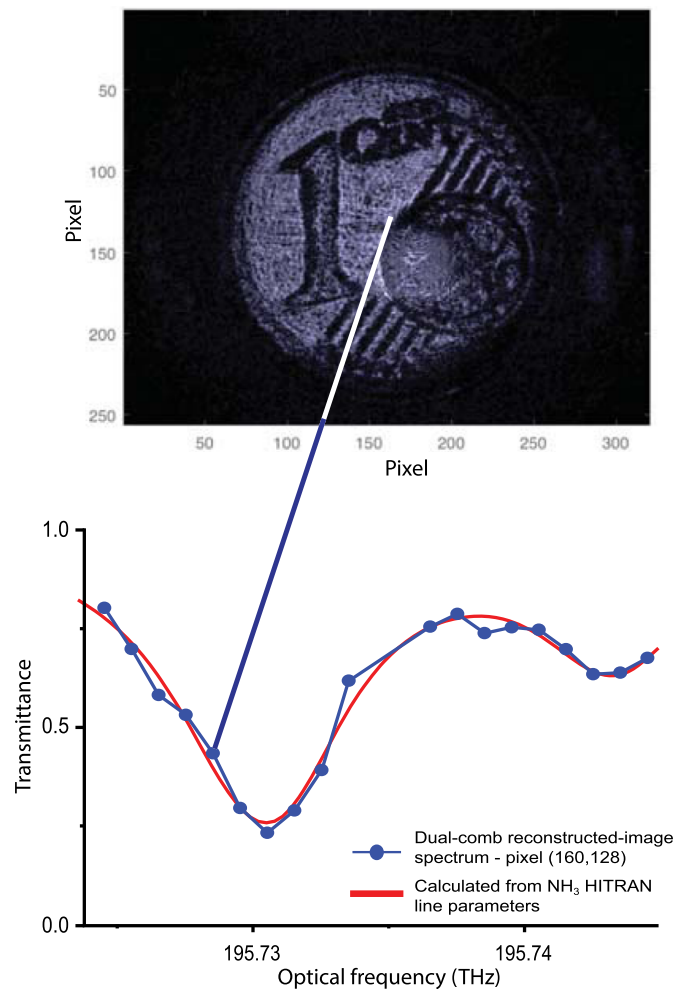


**Extended Data Fig. 1 | Reconstruction of dual-comb holographic amplitude and phase maps of an object in transmission.** The object is a resolution test target (1951 USAF) which works in transmission. The two continuous-wave lasers emit at the respective frequencies of  $f_1 = 194.135$  THz and  $f_2 = 195.405$  THz. The object-comb line spacing is  $f_{\text{rep}} = 1,000$  MHz and the difference in repetition frequencies is  $\delta f_{\text{rep}} = 2$  Hz. The object-comb and the reference-comb each include about 50 lines. The same style of representation as in Fig. 2 is adopted. **(a)** Frames of the interference between the object and reference waves as a function of time on a detector matrix. An interferometric hypercube, consisting of 81,920 pixel-interferograms, is measured within a total measurement time of 3.5 seconds. **(b)** Each pixel-interferogram is Fourier transformed to reveal frequency-domain amplitude and phase spectra with resolved comb lines. **(c)** As many complex holograms as there are comb lines are obtained. **(d)** At a given frequency, an inverse Fresnel transform of the holograms generates amplitude and phase images over the entire range of focal distances. The amplitude image and the phase map of the resolution test target in focus are shown at right.



Extended Data Fig. 2 | See next page for caption.

**Extended Data Fig. 2 | Robustness of dual-comb holography against missing pixels.** (a) The complex (amplitude and phase) hologram at 195.351 THz is inverse Fourier transformed. At a focusing distance of 0.697 m, the reconstructed amplitude and phase images of a \$1 (€) coin are at focus. (b) The same complex hologram as in (a) is truncated: The samples for 10 entire horizontal pixel lines and 10 entire vertical pixel lines, in the middle of the detector matrix, are arbitrarily set to zero to provide a drastic simulation of the effect of faulty pixels. Nonetheless, the reconstructed images (also at 0.697 m) still provide a recognizable representation of the coin. This robustness is a well-known characteristic of the digital holography technique.



**Extended Data Fig. 3 | Hyperspectral imaging data associated to the 3D image of the phase map in Fig. 5.** The comb repetition frequency is  $f_{\text{rep}} = 1,000 \text{ Hz}$ . Compared to the spectrum shown in Fig. 4, one can observe that the absorption line of ammonia is not as densely sampled. Nevertheless, the absorption spectrum and the holographic image reconstruction of the coin, displayed in focus, show high signal-to-noise ratio.